

# Sub-structure Characteristic Mode Analysis of Microstrip Antennas using a Global Multi-trace Formulation

Ran Zhao<sup>1</sup>, Yuyu Lu<sup>2</sup>, Guang Shang Cheng<sup>2</sup>, Wei Zhu<sup>3</sup>, Jun Hu<sup>3</sup>, and Hakan Bagci<sup>4</sup>

<sup>1</sup>Ran Zhao is with the Electrical and Computer Engineering Program, Computer, Electrical, and Mathematical Science and Engineering Division, King Abdullah University of Science and Technology, Thuwal 23955, Saudi Arabia and also with the School of Electronic Science and Engineering, University of Electronic Science and Technology of China (UESTC), Chengdu 611731, China (e-mail: ran.zhao@kaust.edu.sa)

<sup>2</sup>Yuyu Lu and Guang Shang Cheng are with the Information Materials and Intelligent Sensing Laboratory of Anhui Province, Anhui University, Hefei, China, 230601, and also with the Anhui Province Key Laboratory of Target Recognition and Feature Extraction, Lu'an, China, 237010 (email: 157064746@qq.com, gscheng89@ahu.edu.cn).

<sup>3</sup>Wei Zhu and Jun Hu are with the School of Electronic Science and Engineering, University of Electronic Science and Technology of China (UESTC), Chengdu 611731, China (email: happyweiwei@uestc.edu.cn, hujun@uestc.edu.cn).

<sup>4</sup>Hakan Bagci is with the Electrical and Computer Engineering Program, Computer, Electrical, and Mathematical Science and Engineering Division, King Abdullah University of Science and Technology (KAUST), Thuwal 23955, Saudi Arabia (e-mail: hakan.bagci@kaust.edu.sa).

---

\*This work was supported in part by NSFC under Grant 62231007, Grant 62271002, 61901002 and in part by KAUST OSR under Award 2019-CRG8-4056.

## Abstract

A characteristic mode (CM) method that relies on a global multi-trace formulation (MTF) of surface integral equations is proposed to compute the modes and the resonance frequencies of microstrip patch antennas with finite dielectric substrates and ground planes. Unlike the traditional full-structure CM methods, the global MTF allows for implementation of a sub-structure CM method. This is achieved by representing the coupling of the electromagnetic fields on the substrate and ground plane in the form of a numerical Green function matrix, which yields a more compact generalized eigenvalue equation. The resulting sub-structure CM method avoids the cumbersome computation of the multilayered medium Green function (unlike the CM methods that rely on mixed-potential integral equations) and the volumetric discretization of the substrate (unlike the CM methods that rely on volume-surface integral equations), and numerical results show that it is more accurate than full-structure CM methods in predicting the modal behavior of electromagnetic fields on practical microstrip antennas.

**Keywords:** *Characteristic mode analysis, surface integral equations, multi-trace formulation, microstrip patch antenna.*

# 1 Introduction

Atypical microstrip antenna consists of a metallic patch, a dielectric substrate that supports the patch, and a ground plane which the dielectric substrate is mounted to. Microstrip antennas and antenna arrays with microstrip elements are widely used in wireless systems since they are compact, lightweight, can be easily mounted on different types of surfaces, and their fabrication is relatively straightforward and often cheap [1]. Methods that can compute the modes and the resonance frequencies of a microstrip antenna are indispensable in the design process. To this end, several analytical methods have been developed, including transmission line [2,3] and cavity [3,4] methods. However, it is difficult or even impossible to extend these analytical methods to account for antennas with irregular shapes or thick substrates. For such cases, characteristic mode analysis (CMA), which often relies on numerical modeling of an antenna, can be used to generate the modes and the resonance frequencies required by the design process [5].

CMA has first been applied to perfect electrically conducting (PEC) objects numerically modeled using scattering matrices [6] and surface integral equations (SIEs) [7]. Later, it has been extended to account for dielectric and composite objects that are modeled using SIEs or volume integral equations (VIEs) [8–14]. These methods compute the characteristic modes (CMs) that are supported by the whole structure (which is accessible), and they are termed “full-structure CM” methods in the literature. Another group of methods, which are developed to compute CMs and termed “sub-structure CM” methods, first decompose the object into two regions (accessible feeding region and non-accessible coupling region), then reduce the generalized eigenvalue equation into a more compact form. This is done by re-expressing discretized electromagnetic field interactions in the non-accessible region as a “numerical Green function matrix” [15]. The sub-structure CM methods might be preferred in the design process of microstrip antennas since they directly provide the mode information

supported by the radiation patch and the feeding region [16].

The idea of sub-structure CMA has first been developed for PEC objects [17]. Since then, it has been extended to account for a PEC object in the presence of a dielectric object, and vice-versa [18]. Note that, the CM method, which relies on the mixed-potential integral equation (MPIE) to model microstrip patch antennas [19,20], can also be grouped as a sub-structure CM method, because the electromagnetic field interactions associated with the dielectric substrate and the metallic ground plane are accounted for using the multilayered medium Green function (under the assumption that the substrate and ground plane extend to infinity in transverse direction).

The orthogonality properties of the sub-structure CMs have been discussed in [21] and the differences between the full-structure and sub-structure CMs have been studied in [22] by replacing the substrate with air and simplifying the original composite objects into PEC objects. To compute the modes of practical microstrip patch antennas (with finite substrates and ground planes), a sub-structure CM method that relies on a volume-surface integral equation (VSIE) has been developed [23]. It has been shown that this method leads to an antenna design with a better performance than that is obtained via the traditional full-structure CM methods [16]. To avoid the high computational cost that comes with the volumetric discretization, a sub-structure CM method that relies only on SIEs has been developed to compute the modes of a dielectric resonator antenna with a finite ground plane [24]. However, this method calls for selection of a special weighting matrix to suppress the spurious (non-physical) modes that contaminate the actual CMs of the structure.

Another full-structure CM method that relies on the coupled electric field integral equation (EFIE) and Poggio-Miller-Chang-Harrington-Wu-Tsai (PMCHWT) equation [25] has been developed in [26]. However, it is not trivial to transform this method into a sub-structure CM method. This is because the equivalent surface currents introduced on the metallic and the dielectric surfaces are not naturally separated. Fortunately, the global

multi-trace formulation (MTF) developed in [27] to analyze electromagnetic scattering from a dielectric object partially covered with a metallic sheet, can be adopted to alleviate this bottleneck. This method introduces a virtual gap to separate the adjacent metallic and dielectric domains.

In this work, first, the global MTF presented in [27] is carefully derived and it is used to develop a sub-structure CM equation to numerically characterize the modes and the resonance frequencies of practical microstrip patch antennas with finite substrates and ground planes. Note that in this formulation, radiation patch and its feeding portion are the accessible region (where the modes are computed) and the substrate and the ground plane are the non-accessible region. Having said that, the effects of the electromagnetic field interactions on the non-accessible region are fully accounted for, which can be interpreted as constructing and using a numerical Green function. Numerical results demonstrate that the proposed method can accurately predict the modal behavior of the electromagnetic fields and the associated resonance frequencies on practical microstrip antennas.

## 2 Formulation

### 2.1 Global MTF

Consider a dielectric object partially covered by an infinitesimally thin PEC sheet as shown in Fig. 1(a). This composite structure resides in an unbounded background medium and is excited by an incident electromagnetic field  $\{\mathbf{E}^i, \mathbf{H}^i\}$ . Let the background medium and the dielectric region be represented by  $\Omega_0$  and  $\Omega_1$ , respectively. The permittivity, the permeability, the wave impedance, and the wave number in  $\Omega_m, m = 0, 1$ , are denoted by  $\varepsilon_m, \mu_m, \eta_m$ , and  $k_m$ , respectively. Let  $S_c$  and  $S_d$  represent the open surface of the PEC sheet and the closed surface of the dielectric object, respectively.

Surfaces  $S_c$  and  $S_d$  are “separated” from each other by introducing an infinitesimally

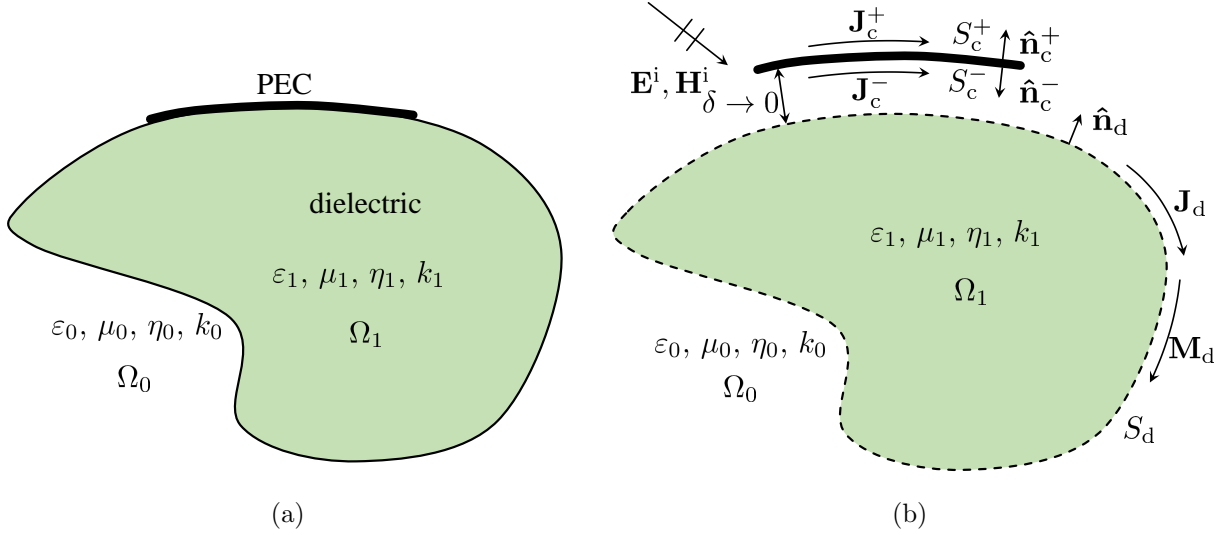


Figure 1: (a) Dielectric object partially covered by a PEC sheet. (b) Equivalent problems.

thin *virtual* gap (same medium as the background) as shown in Fig. 1(b). Different from the formulation described in [27], two sets of equivalent electric currents  $\mathbf{J}_c^+(\mathbf{r})$  and  $\mathbf{J}_c^-(\mathbf{r})$  are defined on the upper side  $S_c^+$  (the side that “touches” the background medium in Fig. 1(a)) and the lower side  $S_c^-$  (the side that “touches” the dielectric object in Fig. 1(a)) of  $S_c$ , respectively. Equivalent electric current  $\mathbf{J}_d(\mathbf{r})$  and the equivalent magnetic current  $\mathbf{M}_d(\mathbf{r})$  are defined on  $S_d$ . In the exterior and interior equivalent problems,  $S_d^+$  and  $S_d^-$  represent the “outer” and the “inner” sides of  $S_d$ , respectively. In Fig. 1(b),  $\hat{\mathbf{n}}_d(\mathbf{r})$ ,  $\hat{\mathbf{n}}_c^+(\mathbf{r})$ , and  $\hat{\mathbf{n}}_c^-(\mathbf{r})$  denote the outward pointing unit normal vectors of  $S_d$ ,  $S_c^+$ , and  $S_c^-$ , respectively.

Let  $\mathcal{L}_m\{\mathbf{X}\}(\mathbf{r})$  and  $\mathcal{K}_m\{\mathbf{X}\}(\mathbf{r})$  represent the integral operators defined as [26]

$$\mathcal{L}_m\{\mathbf{X}\}(\mathbf{r}) = -jk_m \int_S \left( \mathbf{I} + \frac{1}{k_m^2} \nabla \nabla \cdot \right) G_m(\mathbf{r}, \mathbf{r}') \mathbf{X}(\mathbf{r}') ds' \quad (1)$$

$$\begin{aligned} \mathcal{K}_m\{\mathbf{X}\}(\mathbf{r}) &= \int_S \nabla G_m(\mathbf{r}, \mathbf{r}') \times \mathbf{X}(\mathbf{r}') ds' \\ &= \pm \frac{1}{2} \mathbf{X}(\mathbf{r}) \times \hat{\mathbf{n}}(\mathbf{r}) + \bar{\mathcal{K}}_m\{\mathbf{X}\}(\mathbf{r}) \end{aligned} \quad (2)$$

where  $G_m(\mathbf{r}, \mathbf{r}') = e^{-jk_m|\mathbf{r}-\mathbf{r}'|}/(4\pi|\mathbf{r}-\mathbf{r}'|)$  is the Green function of the unbounded medium with permittivity  $\varepsilon_m$  and permeability  $\mu_m$  and  $S$  represent the surface on which  $\mathbf{X}$  is defined. In (2),  $\hat{\mathbf{n}}(\mathbf{r})$  is the outward pointing unit normal vector of  $S$ ,  $\bar{\mathcal{K}}_m\{\mathbf{X}\}(\mathbf{r})$  represents the principle value integral term of  $\mathcal{K}_m\{\mathbf{X}\}(\mathbf{r})$ , and ‘-’ and ‘+’ signs (in front of the residue term) are selected when  $\mathbf{r}$  approaches  $S$  along the direction and the opposite direction of  $\hat{\mathbf{n}}(\mathbf{r})$ , respectively. Note that in the remainder of the paper, the dependence of the variables on  $\mathbf{r}$  is dropped for the sake of simplicity in the notation.

For the exterior equivalent problem, electromagnetic fields and the equivalent currents satisfy

$$\begin{aligned}\mathbf{M}_c^+ &= \frac{1}{\eta_0}(\mathbf{E}^i + \mathbf{E}_0^s) \times \hat{\mathbf{n}}_c^+ = 0, \mathbf{r} \in S_c^+ \\ \mathbf{M}_c^- &= \frac{1}{\eta_0}(\mathbf{E}^i + \mathbf{E}_0^s) \times \hat{\mathbf{n}}_c^- = 0, \mathbf{r} \in S_c^- \\ \mathbf{M}_d &= \frac{1}{\eta_0}(\mathbf{E}^i + \mathbf{E}_0^s) \times \hat{\mathbf{n}}_d, \mathbf{r} \in S_d^+ \\ \mathbf{J}_d &= \hat{\mathbf{n}}_d \times (\mathbf{H}^i + \mathbf{H}_0^s), \mathbf{r} \in S_d^+.\end{aligned}\tag{3}$$

Here,  $\mathbf{E}_0^s$  and  $\mathbf{H}_0^s$  are the scattered electric and magnetic fields in  $\Omega_0$  and expressed in terms of the equivalent currents using [27]

$$\begin{aligned}\mathbf{E}_0^s &= \eta_0(\mathcal{L}_0\{\mathbf{J}_c^+\} + \mathcal{L}_0\{\mathbf{J}_c^-\} + \mathcal{L}_0\{\mathbf{J}_d\} - \mathcal{K}_0\{\mathbf{M}_d\}), \mathbf{r} \in \Omega_0 \\ \mathbf{H}_0^s &= \mathcal{K}_0\{\mathbf{J}_c^+\} + \mathcal{K}_0\{\mathbf{J}_c^-\} + \mathcal{K}_0\{\mathbf{J}_d\} + \mathcal{L}_0\{\mathbf{M}_d\}, \mathbf{r} \in \Omega_0.\end{aligned}\tag{4}$$

Using (3) and (4), and the fact that  $\hat{\mathbf{n}}_c^\pm \times (\mathbf{M}_d \times \hat{\mathbf{n}}_d) \times \hat{\mathbf{n}}_c^\pm = \mathbf{M}_d \times \hat{\mathbf{n}}_d$ ,  $\hat{\mathbf{n}}_d \times (\mathbf{J}_c^\pm \times \hat{\mathbf{n}}_c^\pm) \times \hat{\mathbf{n}}_d = \mathbf{J}_c^\pm \times \hat{\mathbf{n}}_c^\pm$ ,  $\mathbf{r} \in S_c^\pm$ , EFIEs on  $S_c^+$ ,  $S_c^-$ , and  $S_d^+$  and the magnetic field integral equation (MFIE) on  $S_d^+$  can be obtained for the exterior problem as

$$\begin{aligned}\eta_0 \frac{\mathbf{M}_d}{2} \times \hat{\mathbf{n}}_d - \eta_0 \hat{\mathbf{n}}_c^+ \times (\mathcal{L}_0\{\mathbf{J}_c^+\} + \mathcal{L}_0\{\mathbf{J}_c^-\} \\ + \mathcal{L}_0\{\mathbf{J}_d\} - \bar{\mathcal{K}}_0\{\mathbf{M}_d\}) \times \hat{\mathbf{n}}_c^+ = \hat{\mathbf{n}}_c^+ \times \mathbf{E}^i \times \hat{\mathbf{n}}_c^+, \mathbf{r} \in S_c^+\end{aligned}\tag{5}$$

$$\begin{aligned} & \eta_0 \frac{\mathbf{M}_d}{2} \times \hat{\mathbf{n}}_d - \eta_0 \hat{\mathbf{n}}_c^- \times (\mathcal{L}_0\{\mathbf{J}_c^+\} + \mathcal{L}_0\{\mathbf{J}_c^-\}) \\ & + \mathcal{L}_0\{\mathbf{J}_d\} - \bar{\mathcal{K}}_0\{\mathbf{M}_d\}) \times \hat{\mathbf{n}}_c^- = \hat{\mathbf{n}}_c^- \times \mathbf{E}^i \times \hat{\mathbf{n}}_c^-, \mathbf{r} \in S_c^- \end{aligned} \quad (6)$$

$$\begin{aligned} & \eta_0 \hat{\mathbf{n}}_d \times \frac{\mathbf{M}_d}{2} - \eta_0 \hat{\mathbf{n}}_d \times (\mathcal{L}_0\{\mathbf{J}_c^+\} + \mathcal{L}_0\{\mathbf{J}_c^-\}) \\ & + \mathcal{L}_0\{\mathbf{J}_d\} - \bar{\mathcal{K}}_0\{\mathbf{M}_d\}) \times \hat{\mathbf{n}}_d = \hat{\mathbf{n}}_d \times \mathbf{E}^i \times \hat{\mathbf{n}}_d, \mathbf{r} \in S_d^+ \end{aligned} \quad (7)$$

$$\begin{aligned} & \eta_0 \frac{\mathbf{J}_d}{2} \times \hat{\mathbf{n}}_d + \eta_0 \frac{\mathbf{J}_c^+}{2} \times \hat{\mathbf{n}}_c^+ - \eta_0 \frac{\mathbf{J}_c^-}{2} \times \hat{\mathbf{n}}_c^- \\ & - \eta_0 \hat{\mathbf{n}}_d \times (\bar{\mathcal{K}}_0\{\mathbf{J}_c^+\} + \bar{\mathcal{K}}_0\{\mathbf{J}_c^-\} + \mathcal{L}_0\{\mathbf{M}_d\} \\ & + \bar{\mathcal{K}}_0\{\mathbf{J}_d\}) \times \hat{\mathbf{n}}_d = \eta_0 \hat{\mathbf{n}}_d \times \mathbf{H}^i \times \hat{\mathbf{n}}_d, \mathbf{r} \in S_d^+. \end{aligned} \quad (8)$$

Because  $S_c$  is an open surface and  $\hat{\mathbf{n}}_c^- \times \mathbf{A} \times \hat{\mathbf{n}}_c^- = \hat{\mathbf{n}}_c^+ \times \mathbf{A} \times \hat{\mathbf{n}}_c^+$  for any vector  $\mathbf{A}$ , (5) and (6) are equivalent to each other and they can be merged into a single equation by defining a new electric current as the collection of  $\mathbf{J}_c^+$  and  $\mathbf{J}_c^-$ , i.e.,  $\mathbf{J}_c = \mathbf{J}_c^+ \cup \mathbf{J}_c^-$ . Noting that  $\hat{\mathbf{n}}_d = \pm \hat{\mathbf{n}}_c^\pm$ ,  $\mathbf{r} \in S_c^\pm$ , this new equation can be written as

$$\begin{aligned} & \eta_0 \frac{\mathbf{M}_d}{2} \times \hat{\mathbf{n}}_d - \eta_0 \hat{\mathbf{n}}_d \times (\mathcal{L}_0\{\mathbf{J}_c\} + \mathcal{L}_0\{\mathbf{J}_d\} \\ & - \bar{\mathcal{K}}_0\{\mathbf{M}_d\}) \times \hat{\mathbf{n}}_d = \hat{\mathbf{n}}_d \times \mathbf{E}^i \times \hat{\mathbf{n}}_d, \mathbf{r} \in S_c. \end{aligned} \quad (9)$$

Using  $\mathbf{J}_c = \mathbf{J}_c^+ \cup \mathbf{J}_c^-$  in (7) yields

$$\begin{aligned} & \eta_0 \hat{\mathbf{n}}_d \times \frac{\mathbf{M}_d}{2} - \eta_0 \hat{\mathbf{n}}_d \times (\mathcal{L}_0\{\mathbf{J}_c\} + \mathcal{L}_0\{\mathbf{J}_d\} \\ & - \bar{\mathcal{K}}_0\{\mathbf{M}_d\}) \times \hat{\mathbf{n}}_d = \hat{\mathbf{n}}_d \times \mathbf{E}^i \times \hat{\mathbf{n}}_d, \mathbf{r} \in S_d^+. \end{aligned} \quad (10)$$

Similarly, using  $\mathbf{J}_c = \mathbf{J}_c^+ \cup \mathbf{J}_c^-$  and  $\hat{\mathbf{n}}_c^+ = -\hat{\mathbf{n}}_c^-$  in (8) yields

$$\begin{aligned} & \eta_0 \frac{\mathbf{J}_d + \mathbf{J}_c}{2} \times \hat{\mathbf{n}}_d - \eta_0 \hat{\mathbf{n}}_d \times (\bar{\mathcal{K}}_0\{\mathbf{J}_c\} + \mathcal{L}_0\{\mathbf{M}_d\} \\ & + \bar{\mathcal{K}}_0\{\mathbf{J}_d\}) \times \hat{\mathbf{n}}_d = \eta_0 \hat{\mathbf{n}}_d \times \mathbf{H}^i \times \hat{\mathbf{n}}_d, \mathbf{r} \in S_d^+. \end{aligned} \quad (11)$$

Note that  $\hat{\mathbf{n}}_d \times \mathbf{M}_d = 0$ ,  $\mathbf{r} \in S_c \cap S_d^+$ , since  $S_c$  is a PEC surface. The same boundary condition can be obtained by subtracting (9) from (10).

For the interior equivalent problem, electromagnetic fields and the equivalent currents satisfy

$$\begin{aligned} -\mathbf{M}_d &= \frac{1}{\eta_0} \mathbf{E}_1^s \times (-\hat{\mathbf{n}}_d), \mathbf{r} \in S_d^- \\ -\mathbf{J}_d &= (-\hat{\mathbf{n}}_d) \times \mathbf{H}_1^s, \mathbf{r} \in S_d^- \end{aligned} \quad (12)$$

where  $\mathbf{E}_1^s$  and  $\mathbf{H}_1^s$  are the scattered electric and magnetic fields in  $\Omega_1$  and expressed in terms of the equivalent currents using [27]

$$\begin{aligned} \mathbf{E}_1^s &= \eta_1 \mathcal{L}_1 \{\mathbf{J}_d\} - \eta_0 \mathcal{K}_1 \{\mathbf{M}_d\}, \mathbf{r} \in \Omega_1 \\ \mathbf{H}_1^s &= \mathcal{K}_1 \{\mathbf{J}_d\} + \frac{\eta_0}{\eta_1} \mathcal{L}_1 \{\mathbf{M}_d\}, \mathbf{r} \in \Omega_1. \end{aligned} \quad (13)$$

Using (12) and (13), one can obtain EFIE and MFIE on  $S_d^-$  for the interior problem as

$$\begin{aligned} \eta_0 \hat{\mathbf{n}}_d \times \frac{\mathbf{M}_d}{2} + \hat{\mathbf{n}}_d \times (\eta_1 \mathcal{L}_1 \{\mathbf{J}_d\} - \eta_0 \bar{\mathcal{K}}_1 \{\mathbf{M}_d\}) \times \hat{\mathbf{n}}_d \\ = 0, \mathbf{r} \in S_d^- \end{aligned} \quad (14)$$

$$\begin{aligned} \eta_0 \frac{\mathbf{J}_d}{2} \times \hat{\mathbf{n}}_d + \hat{\mathbf{n}}_d \times (\eta_0 \bar{\mathcal{K}}_1 \{\mathbf{J}_d\} + \frac{\eta_0^2}{\eta_1} \mathcal{L}_1 \{\mathbf{M}_d\}) \times \hat{\mathbf{n}}_d \\ = 0, \mathbf{r} \in S_d^-. \end{aligned} \quad (15)$$

Subtracting (14) from (10) and subtracting (15) from (11) yield two equations on  $S_d$  as

$$\begin{aligned} \hat{\mathbf{n}}_d \times (-\eta_0 \mathcal{L}_0 \{\mathbf{J}_d\} - \eta_1 \mathcal{L}_1 \{\mathbf{J}_d\} + \eta_0 \bar{\mathcal{K}}_0 \{\mathbf{M}_d\} \\ + \eta_0 \bar{\mathcal{K}}_1 \{\mathbf{M}_d\} - \eta_0 \mathcal{L}_0 \{\mathbf{J}_c\}) \times \hat{\mathbf{n}}_d \\ = \hat{\mathbf{n}}_d \times \mathbf{E}^i \times \hat{\mathbf{n}}_d, \mathbf{r} \in S_d \end{aligned} \quad (16)$$

$$\begin{aligned}
& \eta_0 \frac{\mathbf{J}_c}{2} \times \hat{\mathbf{n}}_d + \hat{\mathbf{n}}_d \times \left( -\eta_0 \bar{\mathcal{K}}_0 \{ \mathbf{J}_d \} - \eta_0 \bar{\mathcal{K}}_1 \{ \mathbf{J}_d \} \right. \\
& \left. - \eta_0 \mathcal{L}_0 \{ \mathbf{M}_d \} - \frac{\eta_0^2}{\eta_1} \mathcal{L}_1 \{ \mathbf{M}_d \} - \eta_0 \bar{\mathcal{K}}_0 \{ \mathbf{J}_c \} \right) \times \hat{\mathbf{n}}_d \\
& = \eta_0 \hat{\mathbf{n}}_d \times \mathbf{H}^i \times \hat{\mathbf{n}}_d, \mathbf{r} \in S_d.
\end{aligned} \tag{17}$$

The system of surface integral equations (9), (16), and (17) can be numerically solved for unknown equivalent currents  $\mathbf{J}_c$ ,  $\mathbf{J}_d$ , and  $\mathbf{M}_d$ . First,  $S_c$  and  $S_d$  are discretized into a mesh of triangles. Then,  $\mathbf{J}_c$ ,  $\mathbf{J}_d$ , and  $\mathbf{M}_d$  are expanded using the well-known Rao-Wilton-Glisson (RWG) basis functions, each of which is defined on a pair of triangles [28]. Inserting these expansion into (9), (16), and (17) and applying Galerkin testing to resulting equations yield a matrix system as

$$\begin{aligned}
& \begin{bmatrix} \eta_0 \bar{L}_{dd}^0 + \eta_1 \bar{L}_{dd}^1 & -\eta_0 \bar{K}_{dd}^0 - \eta_0 \bar{K}_{dd}^1 & \eta_0 \bar{L}_{dc}^0 \\ \eta_0 \bar{K}_{dd}^0 + \eta_0 \bar{K}_{dd}^1 & \eta_0 \bar{L}_{dd}^0 + \frac{\eta_0^2}{\eta_1} \bar{L}_{dd}^1 & \eta_0 \bar{K}_{dc}^0 + \frac{\eta_0}{2} \bar{S}_{dc} \\ \eta_0 \bar{L}_{cd}^0 & -\eta_0 \bar{K}_{cd}^0 + \frac{\eta_0}{2} \bar{S}_{cd} & \eta_0 \bar{L}_{cc}^0 \end{bmatrix} \\
& \begin{bmatrix} \bar{J}_d \\ \bar{M}_d \\ \bar{J}_c \end{bmatrix} = \begin{bmatrix} \bar{E}_d \\ \eta_0 \bar{H}_d \\ \bar{E}_c \end{bmatrix}.
\end{aligned} \tag{18}$$

Here, the unknown coefficients of the basis function sets used to expand  $\mathbf{J}_c$ ,  $\mathbf{J}_d$ , and  $\mathbf{M}_d$  are stored in vectors  $\bar{J}_c$ ,  $\bar{J}_d$ , and  $\bar{M}_d$ , respectively. Vectors  $\bar{E}_d$ ,  $\bar{H}_d$ , and  $\bar{E}_c$  store tested incident fields and matrix blocks  $\bar{L}_{ab}^m$ ,  $\bar{K}_{ab}^m$ , and  $\bar{N}_{ab}^m$ ,  $a, b \in \{c, d\}$  store tested fields of the basis

functions. Entries of these vectors and matrix blocks are given by

$$\begin{aligned}
\{\bar{E}_a\}_p &= \langle \mathbf{f}_a^p, \mathbf{E}^i \rangle_a \\
\{\bar{H}_a\}_p &= \langle \mathbf{f}_a^p, \mathbf{H}^i \rangle_a \\
\{\bar{\bar{L}}_{ab}^m\}_{p,q} &= -\langle \mathbf{f}_a^p, \mathcal{L}_m \{ \mathbf{f}_b^q \} \rangle_a \\
\{\bar{\bar{K}}_{ab}^m\}_{p,q} &= -\langle \mathbf{f}_a^p, \bar{\mathcal{K}}_m \{ \mathbf{f}_b^q \} \rangle_a \\
\{\bar{\bar{S}}_{ab}\}_{p,q} &= \langle \mathbf{f}_a^p, \mathbf{f}_b^q \times \hat{\mathbf{n}}_d \rangle_a.
\end{aligned} \tag{19}$$

Here, subscripts  $a, b \in \{c, d\}$  attached to a variable mean that the variable is defined on/for surface  $S_a$  or  $S_b$ , the inner product of two vector fields  $\mathbf{u}$  and  $\mathbf{v}$  is defined as  $\langle \mathbf{u}, \mathbf{v} \rangle_a = \int_{S_a} \mathbf{u} \cdot \mathbf{v} ds$ , and  $\mathbf{f}_a^p$  and  $\mathbf{f}_b^q$  represent the  $p$ th testing function and the  $q$ th basis function used to test fields on  $S_a$  and expand unknown currents on  $S_b$ , respectively.

## 2.2 Sub-structure CM Method

To facilitate the sub-structure CMA of a microstrip antenna where the radiation patch is the accessible region, matrix system (18) is brought into a form where the basis expansions of  $\mathbf{J}_c$  on the radiation patch (denoted by surface  $S_r$ ) and the finite ground plane (denoted by surface  $S_g$ ) can clearly be identified:

$$\begin{bmatrix} \bar{\bar{Z}}_{11} & \bar{\bar{Z}}_{12} \\ \bar{\bar{Z}}_{21} & \bar{\bar{Z}}_{22} \end{bmatrix} \begin{bmatrix} \bar{I}_1 \\ \bar{I}_2 \end{bmatrix} = \begin{bmatrix} \bar{V}_1 \\ \bar{V}_2 \end{bmatrix}. \tag{20}$$

Here, subscripts  $r, g$ , and  $d$  attached to a variable mean that the variable is defined on/for surface  $S_r$  (radiation patch) or  $S_g$  (ground plane), and  $S_d$  (dielectric surface), respectively. In (20),  $\bar{I}_1 = [\bar{J}_d \ \bar{M}_d \ \bar{J}_g]^T$  and  $\bar{I}_2 = \bar{J}_r$ , where  $\bar{J}_g$  and  $\bar{J}_r$  store the basis function expansion coefficients of  $\mathbf{J}_c$  on  $S_g$  and  $S_r$ , respectively. Similarly,  $\bar{V}_1 = [\bar{E}_d \ \eta_0 \bar{H}_d \ \bar{E}_g]^T$  and  $\bar{V}_2 = \bar{E}_r$ , where  $\bar{E}_g$  and  $\bar{E}_r$  store the incident fields tested on  $S_g$  and  $S_r$ , respectively. The matrix

blocks  $\bar{\bar{Z}}_{11}$ ,  $\bar{\bar{Z}}_{12}$ ,  $\bar{\bar{Z}}_{21}$ , and  $\bar{\bar{Z}}_{22}$  are given by

$$\begin{aligned}
\bar{\bar{Z}}_{11} &= \begin{bmatrix} \eta_0 \bar{\bar{L}}_{\text{dd}}^0 + \eta_1 \bar{\bar{L}}_{\text{dd}}^1 & -\eta_0 \bar{\bar{K}}_{\text{dd}}^0 - \eta_0 \bar{\bar{K}}_{\text{dd}}^1 & \eta_0 \bar{\bar{L}}_{\text{dg}}^0 \\ \eta_0 \bar{\bar{K}}_{\text{dd}}^0 + \eta_0 \bar{\bar{K}}_{\text{dd}}^1 & \eta_0 \bar{\bar{L}}_{\text{dd}}^0 + \frac{\eta_0^2}{\eta_1} \bar{\bar{L}}_{\text{dd}}^1 & \eta_0 \bar{\bar{K}}_{\text{dg}}^0 + \frac{\eta_0}{2} \bar{\bar{S}}_{\text{dg}} \\ \eta_0 \bar{\bar{L}}_{\text{gd}}^0 & -\eta_0 \bar{\bar{K}}_{\text{gd}}^0 + \frac{\eta_0}{2} \bar{\bar{S}}_{\text{gd}} & \eta_0 \bar{\bar{L}}_{\text{gg}}^0 \end{bmatrix} \\
\bar{\bar{Z}}_{12} &= \left[ (\eta_0 \bar{\bar{L}}_{\text{dr}}^0)^{\text{T}} \quad (\eta_0 \bar{\bar{K}}_{\text{dr}}^0 + \frac{\eta_0}{2} \bar{\bar{S}}_{\text{dr}})^{\text{T}} \quad (\eta_0 \bar{\bar{L}}_{\text{gr}}^0)^{\text{T}} \right]^{\text{T}} \\
\bar{\bar{Z}}_{21} &= \begin{bmatrix} \eta_0 \bar{\bar{L}}_{\text{rd}}^0 & -\eta_0 \bar{\bar{K}}_{\text{rd}}^0 + \frac{\eta_0}{2} \bar{\bar{S}}_{\text{rd}} & \eta_0 \bar{\bar{L}}_{\text{gr}}^0 \end{bmatrix} \\
\bar{\bar{Z}}_{22} &= \eta_0 \bar{\bar{L}}_{\text{rr}}^0.
\end{aligned} \tag{21}$$

To carry out the sub-structure CMA, first, the right hand side  $\bar{V}_1$  of (20) is set to zero, then the first row is inverted for  $\bar{I}_1$ , and the result is inserted into the second row. This yields

$$\underbrace{(\bar{\bar{Z}}_{22} - \bar{\bar{Z}}_{21} (\bar{\bar{Z}}_{11})^{-1} \bar{\bar{Z}}_{12})}_{\bar{\bar{Z}}_{\text{sub}}} \bar{I}_2 = \bar{V}_2 \tag{22}$$

where  $\bar{\bar{Z}}_{21} (\bar{\bar{Z}}_{11})^{-1} \bar{\bar{Z}}_{12}$  is the perturbation matrix. This term is also referred to as the numerical Green function matrix and represents the electromagnetic coupling effects from the dielectric substrate and the ground plane to the radiation patch.

The generalized eigenvalue equation corresponding to the linear system in (22) is given as [17],

$$\bar{\bar{X}}_{\text{sub}} \bar{I}_n = \lambda_n \bar{\bar{R}}_{\text{sub}} \bar{I}_n \tag{23}$$

where  $\lambda_n$  and  $\bar{I}_n$  are the  $n$ th eigenvalue and corresponding eigenvector, and  $\bar{\bar{X}}_{\text{sub}}$  and  $\bar{\bar{R}}_{\text{sub}}$  are the imaginary and the real parts of  $\bar{\bar{Z}}_{\text{sub}}$ , respectively.

### 3 Numerical Results

In this section, three different numerical examples that demonstrate the applicability and the accuracy of the proposed CM method are presented. In all examples, CMA is carried out at frequency samples in a given frequency range, and the resonance frequency is identified as the frequency sample where the eigenvalue  $\lambda_n$  of a mode is closest to zero. This is because eigenvalues may not be exactly zero due to the sampling in frequency and the numerical errors in constructing the matrix system in (20). For each example, the modal significance (MS) is computed using  $MS = 1/|1 + j\lambda_n|$  [7] and is plotted against frequency.

#### 3.1 Rectangular Patch Antenna

In the first numerical example, the rectangular PEC patch of the antenna entirely covers the upper surface of an FR-4 substrate with the length 100 mm, width 40 mm, height 1.55 mm. The substrate is non-magnetic and its relative permittivity is 4.7. The frequency band ranges from 1.0 GHz to 3.0 GHz and is sampled with a step of 25 MHz. The average edge length of the triangular elements discretizing the surfaces of the antenna is 4.0 mm.

First, CMA is carried out using three full-structure CM methods, which rely on the global MTF (eigenvalues of (20) are computed), VSIE as implemented by the commercial software FEKO, and EFIE-PMCHWT as described in [26]. The radiation weighting matrices of generalized eigenvalue equation are chosen following the principle described in [13] to avoid the contamination of the nonphysical modes. Fig. 2(a) plots MS computed by these three methods versus frequency. Clearly, all three results agree well. The resonance frequencies computed by the full-structure CM methods that rely on VSIE and the global MTF are both 1.250 GHz and 2.775 GHz, which verifies the accuracy of the global MTF in full-structure CMA.

Next, the accuracy of the proposed sub-structure CM method that relies on the global

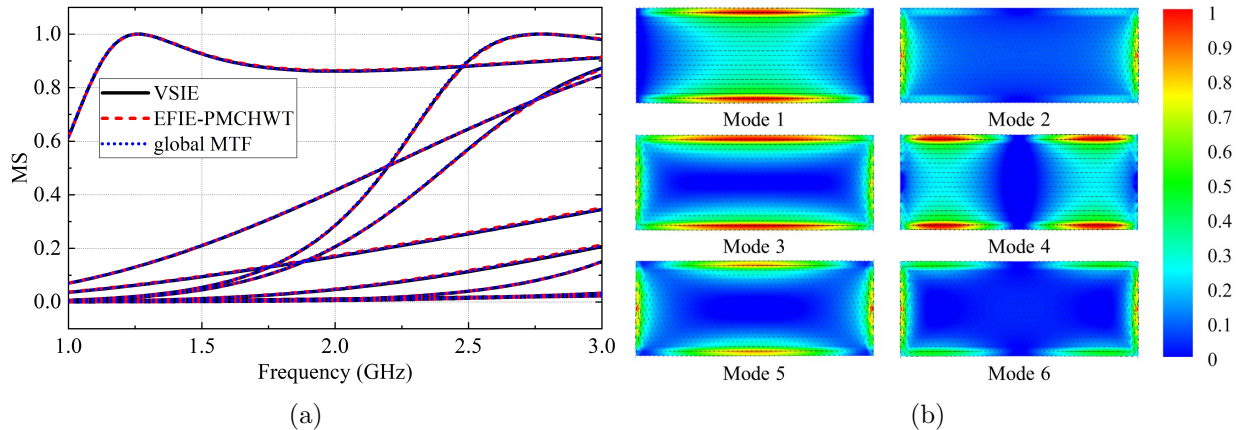


Figure 2: (a) The MS curves of the first 9 full-structure CMs of the rectangular patch antenna. (b) Amplitude of the first 6 electric eigencurrents supported by the PEC patch at 1.275 GHz.

MTF is studied. The first resonance frequency is computed as 1.275 GHz, which is the same value obtained by the sub-structure CM method that relies on VSIE [23]. Fig. 2(b) plots the amplitude of the first 6 electric eigencurrents on the PEC patch of the antenna at 1.275 GHz as obtained by the proposed method. These match the results presented in [23].

### 3.2 Triangular Microstrip Patch antenna

In this example, the antenna consists of a triangular PEC patch, a dielectric substrate, a PEC ground plane as shown in Fig. 3(a). The center of the triangular patch coincides with that of the upper surface of the substrate. The dimensions of the geometry are provided on the figure. The substrate is non-magnetic and its relative permittivity is 2.32. The frequency band ranges from 1.0 GHz to 3.5 GHz and is sampled with a step of 10 MHz. The average edge length of the triangular elements discretizing the surfaces of the antenna is 5 mm.

The MS curves of the first 15 CMs obtained using the proposed sub-structure CM method that relies on the global MTF are plotted in Fig. 3(b). The figure clearly shows the resonance frequencies where MS approaches 1.0 ( $\lambda_n$  approaches 0). Table 1 provides the first 7 resonance frequencies obtained via measurements [29], using the cavity model [30], using the

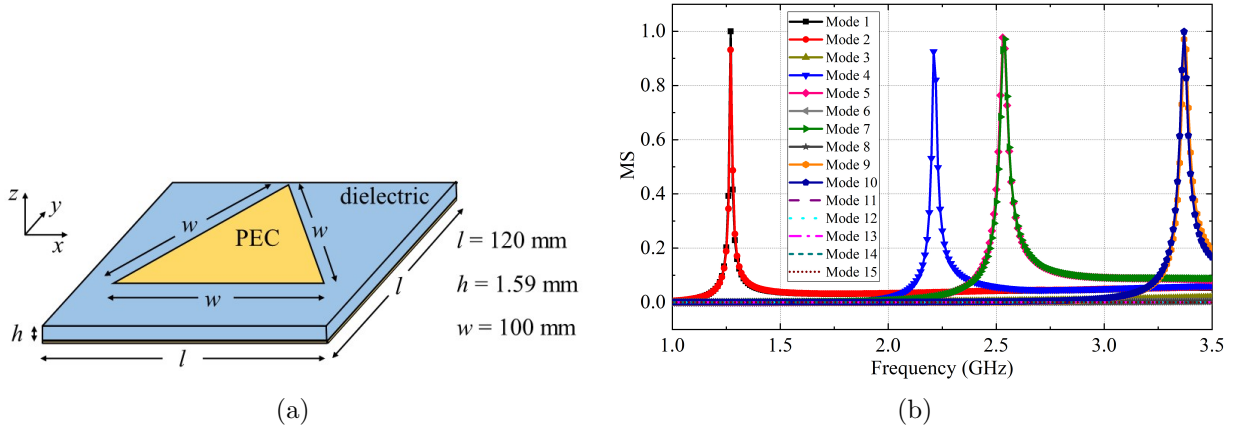


Figure 3: (a) Geometry of the triangular microstrip patch antenna. (b) The MS curves of the first 15 CMs obtained using the proposed sub-structure CM method that relies on the global MTF.

Table 1: Resonance Frequencies (in GHz) of the Triangular Microstrip Patch Antenna

Measured	Cavity model	CM method with MPIE	CM method with MTF
1.28	1.30	1.30	1.27
1.28	1.30	1.30	1.27
2.24	2.25	2.25	2.21
2.55	2.60	2.57	2.53
2.55	2.60	2.57	2.54
3.40	3.44	3.44	3.37
3.40	3.44	3.44	3.37

CM method that relies on MPIE [19], and using the proposed sub-structure CM method that relies on the global MTF. The table clearly shows that the resonance frequencies obtained using the proposed method agree well with those obtained using other methods, including measurements.

### 3.3 Rectangular Microstrip Patch antenna

In the last example, the antenna consists of rectangular PEC patch, a dielectric substrate, and PEC ground plane as shown in Fig. 4(a). The center of rectangular patch coincides with

Table 2: resonance frequencies (in GHz) of the Rectangular Microstrip Patch Antenna

Simulated $S_{11}$	Cavity model	CM method with MPIE	CM method with VSIE	CM method with MTF
1.05	1.08	1.08	1.09	1.06
1.55	1.61	1.60	1.65	1.57
1.90	1.96	1.95	2.03	1.92
2.10	2.15	2.13	2.19	2.10

that of the upper surface of substrate. The dimensions of the geometry are provided on the figure. The substrate is non-magnetic and its relative permittivity is 3.38. The frequency band ranges from 0.8 GHz to 2.2 GHz is sampled with a step of 10 MHz. The average edge length of the triangular elements discretizing the surfaces of the antenna is 6 mm.

The MS curves of the first 10 CMs obtained using the proposed sub-structure CM method that relies on the global MTF are plotted in Fig. 4(b). The resonance frequencies can clearly be identified. Table 2 compares the first 4 resonance frequencies extracted from the simulated  $S_{11}$  data [19], using cavity model [3], using the CM method that relies on MPIE [19], using the sub-structure CM method that relies on VSIE [16], and using the proposed sub-structure CM method that relies on the global MTF. Although all results agree well with each other, one can see that the results obtained using the proposed method are closer to those obtained from the simulated  $S_{11}$  data.

Fig. 4(c) plots the amplitude of the electric eigencurrents on the PEC patch of the antenna at resonance frequencies 1.06 GHz, 1.57 GHz, 1.92 GHz, and 2.10 GHz. These results agree well with those obtained using the CM method that relies on MPIE [19].

## 4 Conclusion

In this work, a sub-structure CM method that relies on the global MTF of SIEs is formulated and implemented to compute the modes and the resonance frequencies of practical microstrip patch antennas with finite dielectric substrates and ground planes. The global MTF naturally

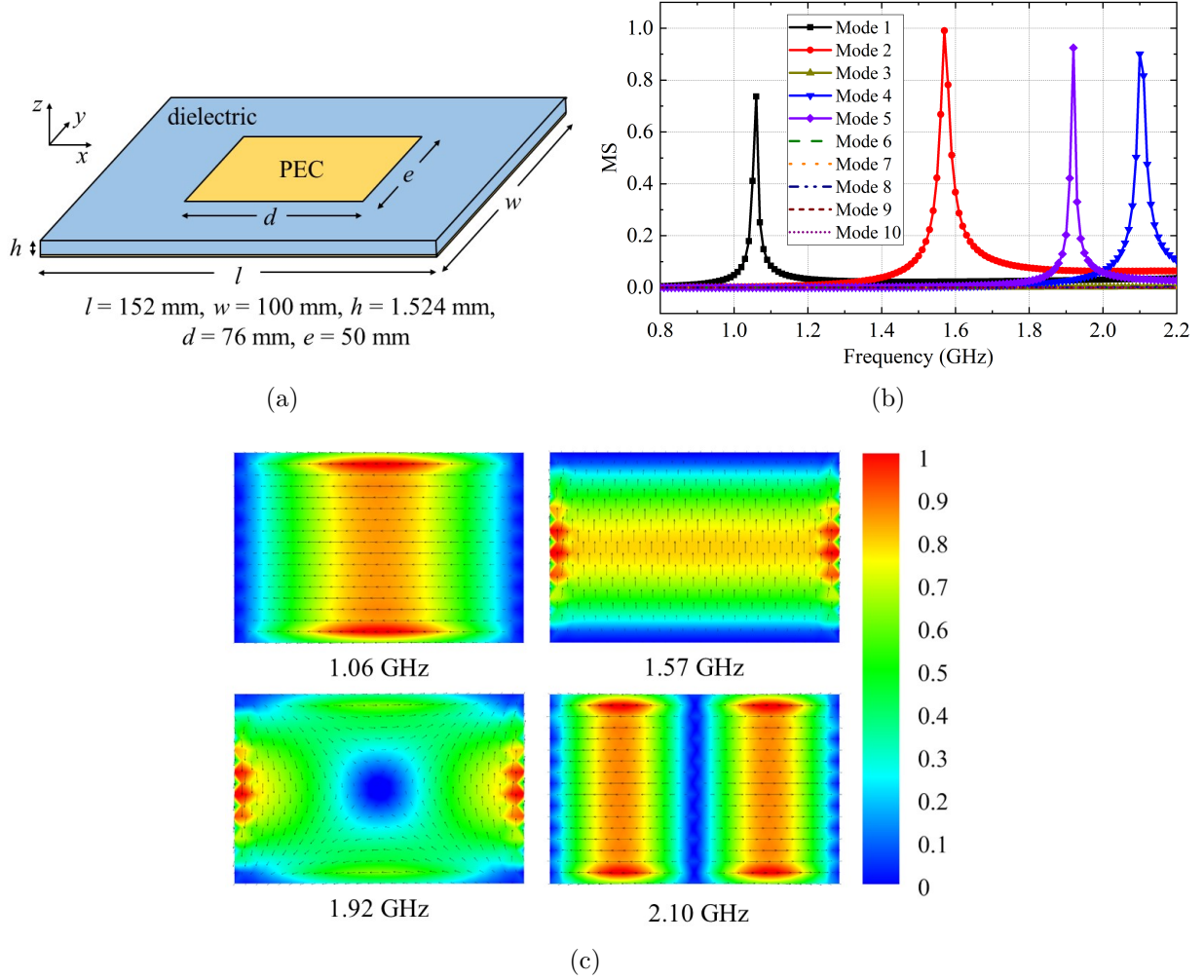


Figure 4: (a) Geometry of the rectangular microstrip patch antenna. (b) The MS curves of the first 10 CMs obtained using the proposed sub-structure CM method that relies on the global MTF. (c) Amplitude of the electric eigencurrents on the PEC patch at resonance frequencies 1.06 GHz, 1.57 GHz, 1.92 GHz, and 2.10 GHz.

separates the equivalent currents on the radiation patch from those on the surfaces of the dielectric substrate, which yields a matrix that can be easily put in a form that is suitable for sub-structure CM analysis. The resulting sub-structure CM method avoids the cumbersome computation of the multilayered medium Green function (unlike the CM methods that rely on MPIE) and the volumetric discretization of the substrate (unlike the CM methods that rely on VSIE), and numerical results show that it is a reliable and accurate approach to

predicting the modal behavior of electromagnetic fields on practical microstrip antennas.

## References

- [1] D. M. Pozar and D. H. Schaubert, *Microstrip Antennas: The Analysis and Design of Microstrip Antennas and Arrays*. John Wiley & Sons, 1995.
- [2] R. Munson, “Conformal microstrip antennas and microstrip phased arrays,” *IEEE Trans. Antennas Propag.*, vol. 22, no. 1, pp. 74–78, 1974.
- [3] Z. N. Chen and M. Y. W. Chia, *Broadband Planar Antennas: Design and Applications*. John Wiley & Sons, 2006.
- [4] D. S. Y. Lo and W. Richards, “Theory and experiment on microstrip antennas,” *IEEE Trans. Antennas Propag.*, vol. 27, no. 2, pp. 137–145, 1979.
- [5] R. Garbacz and D. Pozar, “Antenna shape synthesis using characteristic modes,” *IEEE Trans. Antennas Propag.*, vol. 30, no. 3, pp. 340–350, 1982.
- [6] R. J. Garbacz and R. Turpin, “A generalized expansion for radiated and scattered fields,” *IEEE Trans. Antennas Propag.*, vol. 19, no. 3, pp. 348–358, 1971.
- [7] R. F. Harrington and J. R. Mautz, “Theory of characteristic modes for conducting bodies,” *IEEE Trans. Antennas Propag.*, vol. 19, no. 5, pp. 622–628, 1971.
- [8] J. R. M. R. F. Harrington and Y. Chang, “Characteristic modes for dielectric and magnetic bodies,” *IEEE Trans. Antennas Propag.*, vol. 20, no. 2, pp. 194–198, 1972.
- [9] Y. Chang and R. F. Harrington, “A surface formulation for characteristic modes of material bodies,” *IEEE Trans. Antennas Propag.*, vol. 25, no. 6, pp. 789–795, 1977.

- [10] R. Lian, J. Pan, and S. Huang, “Alternative surface integral equation formulations for characteristic modes of dielectric and magnetic bodies,” *IEEE Transactions on Antennas and Propagation*, vol. 65, no. 9, pp. 4706–4716, 2017.
- [11] F.-G. Hu and C.-F. Wang, “Integral equation formulations for characteristic modes of dielectric and magnetic bodies,” *IEEE Transactions on Antennas and Propagation*, vol. 64, no. 11, pp. 4770–4776, 2016.
- [12] L. Guo, Y. Chen, and S. Yang, “Characteristic mode formulation for dielectric coated conducting bodies,” *IEEE Transactions on Antennas and Propagation*, vol. 65, no. 3, pp. 1248–1258, 2017.
- [13] P. Ylä-Oijala, “Generalized theory of characteristic modes,” *IEEE Transactions on Antennas and Propagation*, vol. 67, no. 6, pp. 3915–3923, 2019.
- [14] M. Kuosmanen, P. Ylä-Oijala, J. Holopainen, and V. Viikari, “Orthogonality properties of characteristic modes for lossy structures,” *IEEE Transactions on Antennas and Propagation*, vol. 70, no. 7, pp. 5597–5605, 2022.
- [15] P. Parhami, Y. Rahmat-Samii, and R. Mittra, “Technique for calculating the radiation and scattering characteristics of antennas mounted on a finite ground plane,” *Proc. Inst. Elect. Eng.*, vol. 124, no. 11, pp. 1009–1016, 1977.
- [16] S. Huang, M.-C. Tang, and C.-F. Wang, “Accurate modal analysis of microstrip patch antennas using sub-structure characteristic modes,” in *2021 International Applied Computational Electromagnetics Society (ACES-China) Symposium*. IEEE, 2021, pp. 1–2.
- [17] J. L. T. Ethier and D. A. McNamara, “Sub-structure characteristic mode concept for antenna shape synthesis,” *Electron. Lett.*, vol. 48, no. 9, pp. 471–472, 2012.

- [18] J. L. T. E. H. Alroughani and D. A. McNamara, "On the classification of characteristic modes, and the extension of sub-structure modes to include penetrable material," in *Proc. Intern. Conf. Electromag. Adv. Appl.*, 2014, pp. 159–162.
- [19] Y. Chen and C. F. Wang, *Characteristic Modes: Theory and Applications in Antenna Engineering*. John Wiley & Sons, 2015.
- [20] M. Meng and Z. Nie, "Study on characteristic mode analysis of three-dimensional conducting objects in lossless layered medium," *IEEE Access*, vol. 6, pp. 77 606–77 614, 2018.
- [21] H. Alroughani, J. Ethier, and D. A. McNamara, "Orthogonality properties of sub-structure characteristic modes," *Microwave and Optical Technology Letters*, vol. 58, no. 2, pp. 481–486, 2016.
- [22] S. Xiang and B. K. Lau, "Preliminary study on differences between full-and sub-structure characteristic modes," in *2019 IEEE International Symposium on Antennas and Propagation and USNC-URSI Radio Science Meeting*. IEEE, 2019, pp. 1863–1864.
- [23] Q. Wu, "General metallic-dielectric structures: A characteristic mode analysis of general metallic-dielectric structures using volume-surface formulations," *IEEE Antennas Propag. Mag.*, vol. 61, no. 3, pp. 27–36, 2019.
- [24] S. Huang, C.-F. Wang, J. Pan, and D. Yang, "Accurate sub-structure characteristic mode analysis of dielectric resonator antennas with finite ground plane," *IEEE Transactions on Antennas and Propagation*, vol. 69, no. 10, pp. 6930–6935, 2021.
- [25] W.-J. Zhao, L.-W. Li, and K. Xiao, "Analysis of electromagnetic scattering and radiation from finite microstrip structures using an efie-pmchwt formulation," *IEEE Transactions on Antennas and Propagation*, vol. 58, no. 7, pp. 2468–2473, 2010.

- [26] K. Fan, R. Zhao, G. Cheng, Z. Huang, and J. Hu, “A spurious-free characteristic mode formulation based on surface integral equation for patch antenna structures,” *IEEE Antennas and Wireless Propagation Letters*, vol. 21, no. 4, pp. 685–689, 2022.
- [27] S. Lasisi, T. Benson, G. Gradoni, M. Greenaway, and K. Cools, “A fast converging resonance-free global multi-trace method for scattering by partially coated composite structures,” *IEEE Transactions on Antennas and Propagation*, 2022.
- [28] D. R. W. S. M. Rao and A. W. Glisson, “Electromagnetic scattering by surfaces of arbitrary shape,” *IEEE Trans. Antennas Propag.*, vol. 30, no. 3, pp. 409–418, 1982.
- [29] J. S. Dahele and K. F. Lee, “Experimental study of the triangular microstrip antenna,” in *Proc. IEEE Int. Symp. Antennas Propag.*, 1984, pp. 283–286.
- [30] K. F. Lee, K. M. Luk, and J. S. Dahele, “Characteristics of the equilateral triangular patch antenna,” *IEEE Trans. Antennas Propag.*, vol. 36, no. 11, pp. 1510–1518, 1988.